Shock Capturing Data Assimilation Algorithm for 1D Shallow Water Equations

Seshu Tirupathi[a,*], Tigran Tchrakian[a], Sergiy Zhuk[a], Sean McKenna[a]

[a] *IBM Research - Ireland, Damastown Industrial Park, Dublin 15, Ireland*

Abstract

We propose a new data assimilation algorithm for shallow water equations in one dimension. The algorithm is based upon Discontinuous Galerkin spatial discretisation of shallow water equations (DG-SW model) and the continuous formulation of the minimax filter. The latter allows for construction of a robust estimation of the state of the DG-SW model and computes worst-case bounds for the estimation error, provided the uncertain parameters belong to a given bounding set. Numerical studies show that, given sparse observations from numerical or physical experiments, the proposed algorithm quickly reconstructs the true solution even in the presence of shocks, rarefaction waves and unknown values of model parameters. The minimax filter is compared against the ensemble Kalman filter (EnKF) for a benchmark dam-break problem and the results show that the minimax filter converges faster to the true solution for sparse observations.

Keywords: Data assimilation, Discontinuous Galerkin, Minimax filter, Shallow water equations

1. Introduction

For modeling of dynamic flooding events where it is important to capture the details of the water level evolution and the transient changes in water flux,

*Corresponding author

Email addresses: seshutir@ie.ibm.com (Seshu Tirupathi), tigran@ie.ibm.com (Tigran Tchrakian), sergiy.zhuk@ie.ibm.com (Sergiy Zhuk), seanmcke@ie.ibm.com (Sean McKenna)

it is necessary to solve the complete shallow-water equations including the acceleration and momentum terms. Such solutions enable accurate simulation of super-critical flows and hydraulic jumps in situations encountered downstream of dam breaks and/or within complex flow geometries. In simulating a variety of 2D test cases, the 18 models compared in [1] predominantly use finite difference or finite volume numerical schemes to solve the shallow water equations. Those models are designed to simulate super-critical flows and capture shocks, of which finite-volume Godunov-type formulations were able to accurately capture time-varying water depths and velocities.

Finite-volume discretization with a Godunov formulation allows for representing water levels as piecewise constant across elements and with discontinuities between elements. This formulation is advantageous in capturing the sharp fronts describing flood waves and rapid changes in fluxes along or across a flooded domain. However, these approaches are generally first-order accurate, so reconstruction procedures like Essentially non-oscillatory (ENO) and Weighted ENO (WENO) need to be employed to make the methods high order [2].

More recently, discontinuous Galerkin (DG) methods have been used to solve the Shallow Water Equations (SWE). DG schemes use a discretization of the SWEs that accounts for strong contrasts in the solution between elements, thus allowing the capture of sharp fronts and transient shocks within the system. Kesserwani and Wang [3] compare the use of a local DG formulation against a finite-volume approach for solving the SWEs for a range of problems including oscillatory flow and one- and two-dimensional inundation problems. They conclude that the DG approach can provide increased accuracy relative to the finite-volume scheme, but at increased complexity.

To date, flood modeling has generally been considered a boundary value problem with boundary conditions typically specified as a time varying water level (hydrograph), driving the inundation across the domain. More recently, the ability to update the model with observational data within the domain has gained interest. In particular, data assimilation for the SWEs has recently

focused on incorporation of satellite imagery into flood models using a variety of assimilation schemes including ensemble Kalman filters, particle filtering, and 4-D variational approaches ([4, 5, 6]). Satellite altimeters can provide timely data on water levels across large areas, albeit at relatively coarse resolution, for input to inundation models. The scale of these approaches dictates that fine-scale details of the flood advance are not resolved and momentum and acceleration terms are not considered in the solution. Assimilation techniques are also amenable to other types of sensor data, for example, [7] simulated river flows with a 2D finite-element model and assimilated Lagrangian data obtained from the tracks of GPS equipped drifters using an ensemble Kalman filter. In [8] a comparison of two data assimilation algorithms for smooth solutions of SWEs (offline optimisation technique based on linearization versus ensemble Kalman filter) was suggested. There have been other approaches where the SWE were simplified to a diffusive model and used to estimate unknown Manning coefficient [9] and make the system robust to abrupt parameter changes and topographic errors [10].

In contrast to the algorithms considered in the above cited works, the data assimilation algorithm of this paper possesses the following distinct features:

- shock capturing,
- flexible uncertainty description in the form of a bounding set,
- a posteriori bounding set enclosing the truth.

We discretize the SWEs in space by means of DG scheme outlined in [11]. This allows us to construct a DG-SW model representing dynamics of the projection coefficients in the Legendre basis. The min-mod slope limiter is applied in the postprocessing cycle in order to allow for shock capturing. The continuous-in-time DG-SW model is then used as a starting point to build a data assimilation algorithm. We refer the reader to section 2 for the detailed discussion.

Note that algorithms based on 4D-Var (or maximum likelihood estimator for PDEs) or ensemble Kalman filter rely on a Gaussian assumption on uncertain

additive model errors, observation noises and initial conditions. In fact, this assumption is built into the definition of the Markov diffusion process [12] and is quite natural for the case of full knowledge of the underlying dynamics (the "drifts" used in MCMC methods). The Gaussian assumption on uncertainties implies that the Markov diffusion process itself is "locally" Gaussian and is centered at the drift with covariance defined by the corresponding characteristics of the additive model error [12]. We stress, however, that in the case considered here, the model error is not an additive one. In contrast, we allow the model itself, the drift, to depend on uncertain parameters (see Section 2) so that we have state dependent model error. We assume that the initial condition and model error are uncertain but bounded and belong to a given bounding set. Statistically, the latter assumption implies uniform distributions for uncertain parameters (see section 3).

The noise in observations, representing time varying water level and velocity data, is assumed to be a realisation of a random process with zero mean and uncertain but bounded covariance matrix in contrast to popular 2nd moment filtering algorithms (for instance, ensemble Kalman filters). The latter assumption is very practical as it makes the data assimilation algorithm robust with respect to fluctuations in the second moments. Under these assumptions, the minimax filter constructs a linear estimate of the DG-SW model's state and produces a bounding set conditioned on the observed data and enclosing the true state of the DG-SW model. Finally, the time integrator used to discretize the filter is a variation of an implicit midpoint method proved to preserve quadratic invariants [13]. Details on minimax filter and the corresponding numerical scheme are provided in Section 3.

Numerical experiments are used to evaluate the accuracy of the proposed data assimilation algorithm in the estimation of time-varying quantities: water levels and momentum. In the first experiment, we present the convergence of the estimated solution to the true solution after setting the variables to an incorrect initial condition (see section 4.1). Observations for this problem are synthetic, namely we generate them by using exact values from the analytical solution

obtained from Riemann initial data. In the second experiment (see section 4.2), we study the convergence of the dependent variables with an unknown model coefficient (Mannings coefficient) and establish the accuracy of the method in capturing the location of the hydraulic jump by comparing it to experimental data. In this case, observations were generated by computing the solution using the correct Mannings coefficient which is proven experimentally to reproduce experimental observations on a sparse (in time) grid.

The work is organized as follows: In section 2, we describe the DG approach to solving the one-dimensional shallow water equations. In Section 3, the theory behind the minimax filter and its use in data assimilation and state estimation are described. Section 4 covers numerical experiments focussed on estimation of final state values from given uncertain initial conditions and comparison of the performance of minimax filter as compared to EnKF filter. This if followed by a numerical experiment to estimation of model parameters considering model error. Conclusions and future work are summarized in Section 5.

2. DG model of St Venant equations

Shallow water equations in one space dimension, also known as St. Venant Equations, are a system of coupled partial differential equations and are represented in conservative form as:

$$\begin{cases} \dfrac{\partial hB}{\partial t} + \dfrac{\partial}{\partial x}\left(huB\right) = 0\,, \\ \dfrac{\partial (huB)}{\partial t} + \dfrac{\partial}{\partial x}\left(hu^2 + \dfrac{1}{2}gh^2B\right) = -ghBS_f\,, \end{cases} \tag{2.1}$$

where h is the water height, u is the velocity of water, B is the width of the domain, g is the gravitational constant and $S_f = \frac{n^2 u|u|}{R^{4/3}}$ is the friction term. The parameters n and R in the friction slope, S_f, are the Manning's roughness coefficient and hydraulic radius (ratio of flow area to the wetted perimeter) respectively. The source term is highly non-linear in h and u since the hydraulic radius is a function of the height of the water surface at any given location. The hydraulic radius in the case of a rectangular channel at any given location x is

given by:

$$R = \frac{h(x)B}{2h(x)+B}\,. \tag{2.2}$$

Substituting R into the friction slope, we get

$$S_f = \frac{n^2 u|u|}{(\frac{hB}{2h+B})^{\frac{4}{3}}}\,, \tag{2.3}$$

In what follows we assume that (2.1) are equipped by appropriate initial conditions and boundary conditions so that the problem is well-posed. Specific examples of boundary and initial conditions will be given in section 4. We refer the reader to [14] for the detailed discussion of the development of discontinuous Galerkin methods for shallow water equations. In what follows we discretize (2.1) in space by using a DG scheme outlined in [11].

The governing equations given in (2.1) can be denoted in simplified form as:

$$U_t + f(U)_x = ST(U)\,; \tag{2.4}$$

where

$$U = \begin{pmatrix} hB \\ huB \end{pmatrix}\,, \quad f(U) = \begin{pmatrix} huB \\ hu^2 + \frac{1}{2}gh^2B \end{pmatrix}\,, \quad ST(U) = \begin{pmatrix} 0 \\ -ghBS_f \end{pmatrix}\,. \tag{2.5}$$

Let us assume that the $1D$ domain, Ω, is discretized into a set of J non-overlapping, conforming cells, given as,

$$\Omega \approx \Omega_h = \bigcup_{j=1}^{J} D^j = \bigcup_{j=1}^{J} [\partial D^{j^-}, \partial D^{j^+}] = \bigcup_{j=1}^{J} [x_{j-\frac{1}{2}}, x_{j+\frac{1}{2}}]\,. \tag{2.6}$$

We approximate the solution U by U_h, where the components of U_h belong to the finite dimensional space of discontinuous piecewise polynomials, $P^k(D^j)$, of degree k in each element. This solution space is denoted as:

$$V = \{v : v|_{D^j} \in P^k(D^j), \quad j = 1, ..., J\}\,. \tag{2.7}$$

Multiplying the governing equations (2.4) with the test function $v \in V$ and integrating by parts, we get for each element,

$$\int_{D^j} \partial_t U v dx - \int_{D^j} f(U)\partial_x v dx + \hat{f}_{j+\frac{1}{2}} v(x^-_{j+\frac{1}{2}}) - \hat{f}_{j-\frac{1}{2}} v(x^+_{j-\frac{1}{2}}) = \int_{D^j} ST(U) v dx \quad \forall v \in V\,, \tag{2.8}$$

where $\hat{f}$ is given by,

$$\hat{f}_{j+\frac{1}{2}} = F(U(x^-_{j+\frac{1}{2}}), U(x^+_{j+\frac{1}{2}}))\,, \tag{2.9}$$

$U(x^+_{j+\frac{1}{2}}) = \lim_{x\downarrow x^+_{j+\frac{1}{2}}} U(x)$, $U(x^-_{j+\frac{1}{2}}) = \lim_{x\uparrow x^-_{j+\frac{1}{2}}} U(x)$, and $F(a_1, a_2)$ is a numerical flux suitably defined to account for stability because of the lack of unique values at the interfaces. In this problem, we take the Lax-Friedrich flux which is given by:

$$F(a_1, a_2) = \frac{1}{2}(f(a_1) + f(a_2) - \alpha(a_2 - a_1))\,, \tag{2.10}$$

where $\alpha = \max(|u| + \sqrt{gh})$. We use Gauss quadrature rules to calculate the integrals given in Eq. (2.8) exactly since the test functions are polynomials in each cell D^j. The minimum number of Gauss quadrature points required to compute the matrix entries exactly is determined by the degree of the polynomials in the integral [15].

Following the general idea of DG methods, it is possible to solve equations (2.8) over each element and communicate the boundary information between the adjacent elements via numerical fluxes (2.10) in the right hand side of (2.8). Method of lines approach is then employed and any explicit time-stepping method can be used to evolve the variables h and hu over time without the need to form a global matrix [16]. However, for the data assimilation purposes (described in the next section) we require the explicit form of the global stiffness matrix. Briefly, the stiffness matrix A is used to evaluate the gain matrix which is used by the state estimator to fuse the model with the sensor data. The governing equations 2.8, can thus be reformulated into a global matrix form as (see Appendix for details):

$$\frac{dU}{dt} = A(U)U + e(U) + b(t)\,, \tag{2.11}$$

where $U : \mathbb{R} \to \mathbb{R}^{N+1}$ and $A : \mathbb{R}^{N+1} \to \mathbb{R}^{N+1}$ is a global stiffness matrix, $e(U)$ is the projection of the state dependent model error depending on the Manning's roughness coefficient (see definition in the appendix), b is the known source term that results from including the contribution of the boundary terms and $N + 1$

is the total number of degrees of freedom (coefficients of the basis functions of U) of the system.

Since the time-evolution of shallow water equations can result in shocks even for smooth initial conditions [11], a slope limiter is required to post-process the solution; this controls the slope component of each element by comparing its of cell average with the cell average of its neighbors. Conservation of mass is preserved by leaving the cell averages unchanged after post-processing. In this paper, we consider a TVD limiter with the standard minmod function m defined as:

$$m(a_1 \cdots a_n) = \begin{cases} s \min_i |a_i| & \text{if } \; s = \text{sign}(a_1) = \cdots = \text{sign}(a_n) \\ 0 & \text{otherwise}\,, \end{cases} \tag{2.12}$$

The DG formulation is fully discretized by choosing a time discretization for the weak form, (2.8).

3. Minimax state estimator

The data assimilation algorithm developed in this paper is based on the minimax state estimation framework. For the convenience of the reader we briefly recall it here. Assume that the state of the process of interest (a vector of projection coefficients in our case) at time instant t is represented by a vector $U(t) \in \mathbb{R}^{N+1}$ and the evolution of $U(t)$ over time is governed by a system of differential equations:

$$\frac{dU}{dt} = A(q)U + e(t) + b(t)\,, \quad U(0) = U_0 + e_0\,, \tag{3.1}$$

where $U_0 \in \mathbb{R}^{N+1}$ is the initial condition (vector of projection coefficients of the initial profile h, hu, see (2.4)), $e(t)$ represents model error, e_0 describes the error in the initial condition, and q is a time-varying parameter. In the following subsection 3.1 we will show that, in fact, q may be a function of the state vector U. In this section, all succeeding derivations are performed assuming that q does not explicitly depend on U. The term $e(t)$ may address either the numerical model error (for instance, projection error introduced by DG method [17]), or

the physical model error, e.g. an error of modelling the river flow by St Venant equations (2.1) introduced by incorrect Manning's roughness coefficients.

In what follows, we assume that e and e_0 are bounded, that is

$$e_0^\top S e_0 + \int_0^T e^\top Q e dt \leq 1\,, \tag{3.2}$$

where S and Q are given symmetric semi-definite matrices. In fact, the above assumption on e_0 and $e(t)$ is natural as the left hand side of (3.2) quantifies the energy of e_0 and $e(t)$ and so (3.2) requires that both physical and projection errors have bounded energy. Clearly, if the energy of $e(t)$ is unbounded then either the discretization is incorrect (infinite numerical error) or the equation (2.1) is not an appropriate model (infinite physical error). Being quite conservative the uncertainty description in terms of an *a priori* ellipsoidal bounding set is aligned with the requirements of our application, as reliable statistics for model errors are often unavailable. The ellipsoidal shape is considered here in order to simplify the presentation. We refer the reader to [18] for more generic convex bounding sets. We refer the reader to [19] for an overview of basic uncertainty quantification methods which may be applied to identify S, Q in practise.

We further assume that the vector of observations, $Y(t)$, is related to the state vector of (3.1), $U(t)$, through the following relation:

$$Y(t) = HU(t) + \eta(t)\,, \tag{3.3}$$

where H is a $M \times (N+1)$-matrix and $\eta(t) \in \mathbb{R}^p$ is the observation error. Here, M is the number of observations and N is the total number of degrees of freedom of U. Recall that vector $U(t)$ approximates modal coefficients of the solution $U(x,t)$ in the Legendre basis. Hence, to evaluate the approximation of the solution at sensor locations, the observation matrix H needs to represent the values of the basis functions, belonging to the element containing the sensor. Thus, the i-th row of H is of the form $(0 \ldots 0, \ldots, 1, x_i, x_i^2, \ldots, x_i^k, 0, \ldots, 0)$ where $x_i \in D^j$ is the location of the ith sensor and the non-zero patch corresponds to the values of Legendre polynomials, forming the basis of the element D^j, at $x_i \in D^j$. DG methods thus provide an added advantage over traditional

finite difference and finite volume methods, namely these methods allow one to naturally map discrete (in space) solution $U(t)$ to any grid representing sensors. In other words, the dicretization for DG-SW model does not depend on sensor locations unlike finite difference and finite volume methods.

Let us now consider the observation error in more detail. We assume that η is a realization of a random process with zero mean and uncertain but bounded correlation operator $K(t) := E\eta(t)\eta^\top(t)$. Note that we do not require the exact representation of K. Instead, as it often happens in practice, we assume that all the second moments of η belong to a given bounding set, namely:

$$\int_0^T \mathrm{trace}(R^{-1}(t)K(t))dt \le 1\,, \tag{3.4}$$

where $R(t)$ is a given symmetric positive definite weighting matrix. The latter assumption is equivalent to the following one:

$$\int_0^T E\eta^\top(t)R^{-1}(t)\eta(t)dt \le 1$$

so that the weighted second moments of the random vector $\eta(t)$, $E\eta^\top(t)R^{-1}(t)\eta(t)$ have bounded energy (as a function of time).

Now, we come to the concept of a minimax estimate. We say that a solution X of (3.1) satisfies uncertainty description (3.2) and (3.4) and X is compatible with the observed realisation of Y if X verifies (3.1)-(3.3) for some (e_0, e) and η such that (e_0, e) satisfies (3.2) and $K(t) := E\eta(t)\eta^\top(t)$ satisfies (3.4). A function $\widehat{\ell^\top U} := \int_0^T \hat{v}^\top(t)Y(t)dt$ is called a minimax estimate of $\ell^\top U(t)$ if

$$E(\ell^\top U(t) - \widehat{\ell^\top U})^2 \le \inf_v \sup_{e,e_0,K} E(\ell^\top U(t) - \int_0^T v^\top(t)Y(t)dt)^2\,,$$

where $\ell \in \mathbb{R}^{N+1}$ and inf is taken over all measurable v. Let us discuss the intuition behind the definition of the minimax estimate. For a given v we may assign a worst-case error $\sigma(v) := \sup_{e,e_0,K} E(\ell^\top U(t) - \int_0^T v^\top(t)Y(t)dt)^2$. In fact, $\sigma(v)$ quantifies the worst-case distance (on average) between a function of observed data, $\int_0^T v^\top(t)Y(t)dt$ and the true value $\ell^\top U(t)$. Clearly, inf operation selects $\hat{v}$ such that $\widehat{\ell^\top U} := \int_0^T \hat{v}^\top(t)Y(t)dt$ has minimal worst-case error. Hence, on average, $\ell^\top U(t) \in \widehat{\ell^\top U} + [-\sigma(v), \sigma(v)]$.

The following lemma suggests one way to compute the minimax estimate and estimation error.

Lemma 1 (see [17]). *Assume that $\widehat{U}(t)$ verifies the following system of ODEs:*

$$\begin{aligned}
&\frac{dB}{dt} = A(p)B + Q^{-1}V\,, B(0) = S^{+}\,,\\
&\frac{dV}{dt} = -A^{\top}(p)V + H^{\top}R^{-1}HB\,, V(0) = I\,,\\
&\frac{d\widehat{U}}{dt} = A(p)\widehat{U} + BV^{-1}H^{\top}R^{-1}(Y(t) - H\widehat{U}(t)) + b(t)\,, \widehat{U}(0) = U_0\,,
\end{aligned} \tag{3.5}$$

Then $\widehat{\ell^{\top}U} = \ell^{\top}\widehat{U}$ and the minimax estimation error is given by:

$$E(\ell^{\top}U(t) - \ell^{\top}\widehat{U}(t))^2 \leq \ell^{\top}B(t)V^{-1}(t)\ell\,, \forall \ell \in \mathbb{R}^{N+1}\,. \tag{3.6}$$

We refer the reader to [20, 21, 22, 18, 23, 24] for the basic information on minimax state estimation framework.

3.1. Non-linear case

As noted, all the derivations above assumed that q does not explicitly depend on U. Formally, we can plug any signal $q(t)$ into (3.5) assuming that it is given a priori. Hence, if we had complete and exact observations of the true state $q(t) := U(t)$, we could plug this q into (3.5) and the result of the above lemma would still be valid. In practice the observations of U are incomplete and noisy and cannot be used directly in (3.5). However, we can still explore this idea by substituting $q(t)$ at time instant t by the estimate of U at time instant t. In this case, the system (3.5) reads as follows:

$$\begin{aligned}
&\frac{dB}{dt} = A(\widehat{U})B + Q^{-1}V\,, B(0) = S^{+}\,,\\
&\frac{dV}{dt} = -A^{\top}(\widehat{U})V + H^{\top}R^{-1}HB\,, V(0) = I\,,\\
&\frac{d\widehat{U}}{dt} = A(\widehat{U})\widehat{U} + BV^{-1}H^{\top}R^{-1}(Y(t) - H\widehat{U}(t)) + b(t)\,, \widehat{U}(0) = U_0\,.
\end{aligned} \tag{3.7}$$

The solvability of the above system can be studied by constructing a convergent sequence of discrete in time approximations and proving that the limiting point

is a unique solution of (3.7). We refer the reader to [25] where such a sequence was constructed for 2D Euler equation which has a similar type of nonlinear convection term. An experimental assessment of (3.7) for scalar conservation laws, specifically macroscopic traffic density models, was presented in [26]. In what follows we describe a possible way of constructing a convergent sequence of discrete in time approximations and provide its numerical assessment in section 4. We stress that the proposed discretisation preserves quadratic invariants. The latter is important as the numerical error estimates are given in terms of a quadratic form (see (3.6)) which needs to be preserved along the trajectories of the discrete filter in order to have worst-case uncertainty bounds valid for the discrete in time system.

We first discretize the DG-SW model to outline the basic idea in the simplest setting. Define $h := \frac{T}{m}$ and assume that U solves $\dot{U} = A(U)U$, $U(0) = U_0$. It then follows that:

$$U((j+1)h) = U(jh) + \int_{jh}^{(j+1)h} A(U(s))U(s)ds$$
$$= U(jh) + \frac{h}{2}\left(A(U(jh))U(jh) + A(U((j+1)h)U((j+1)h))\right) + O(h^3)\,,$$

where the 2nd equality follows from the classical trapezoidal rule, a technique to approximate definite integrals. This suggests a way to compute $U((j+1)h)$ given $U(jh)$. We note that the above approximation is of 2nd order (locally) but it is non-linear in $U((j+1)h)$. Since (3.7) may have discontinuous inputs (generally speaking η is not supposed to be continuous) and so the corresponding solution is at most absolutely continuous we suggest the following 1st order approximation ($j = \overline{1, m-1}$):

$$U((j+1)h) = U(jh) + \frac{h}{2}A(U(jh))(U((j+1)h) + U(jh))\,, U(0) = U_0\,. \quad (3.8)$$

If we now define the Padé transform $P(A) := (I - A)^{-1}(I + A)$ for A with spectral radius $\rho(A) < 1$ and assume that $\|P(A(U(jh)))\|_2 \leq 1$ then: (i) the scheme (3.8) is unconditionally stable for any $h > 0$, and (ii) the vectors $U(jh)$ are bounded as

$$U((j+1)h) = P(\frac{h}{2}A(U(jh)))U(jh) \text{ implies } \|U((j+1)h)\|_2 \leq \|U(0)\|_2\,.$$

Note that $\|P(A(U(jh)))\|_2 \leq 1$ if all the real parts of the eigenvalues of $A(U)$ are negative or $A(U)$ is skew-symmetric. According to the numerical experiments of section 4, the real parts of the eigenvalues of $A(U(jh))$ are negative and hence the condition $\|P(A(U(jh)))\|_2 \leq 1$ holds true.

Now we turn our attention to (3.7). Note that the scheme (3.8) already suggests the use of $U(jh)$ as a value of $q(t)$ at time instant $t = jh$ (see discussion at the very beginning of section 3.1). Following this path we define the following discrete system of equations defining an approximation of the minimax estimate ($j = \overline{1, m-1}$):

$$\begin{aligned}(I - \frac{h}{2}(A(\widehat{U}(jh)) - B_{j,\frac{1}{2}}V^{-1}_{j,\frac{1}{2}}H^\top R^{-1}H))\widehat{U}((j+1)h) \\ =(I + \frac{h}{2}(A(\widehat{U}(jh)) - B_{j,\frac{1}{2}}V^{-1}_{j,\frac{1}{2}}H^\top R^{-1}H))\widehat{U}(jh) + \frac{h}{2}B_{j,\frac{1}{2}}V^{-1}_{j,\frac{1}{2}}Y_{j,\frac{1}{2}} + b_{j,\frac{1}{2}}\end{aligned} \tag{3.9}$$

where $Y_{j,\frac{1}{2}} := Y(j\frac{h}{2})$, $b_{j,\frac{1}{2}} := b(j\frac{h}{2})$ and

$$V_{j,\frac{1}{2}} := \frac{1}{2}(V(jh) + V((j+1)h))\,, B_{j,\frac{1}{2}} := \frac{1}{2}(B(jh) + B((j+1)h))\,.$$

and $B(jh)$ and $V(jh)$ are defined from ($j = \overline{1, m-1}$):

$$\begin{aligned}&\begin{pmatrix} I - \frac{h}{2}A(\widehat{U}(jh)) & Q^{-1} \\ H^\top R^{-1}H & I + \frac{h}{2}A^\top(\widehat{U}(jh)) \end{pmatrix} \begin{bmatrix} B((j+1)h) \\ V((j+1)h) \end{bmatrix} \\ &= \begin{pmatrix} I + \frac{h}{2}A(\widehat{U}(jh)) & Q^{-1} \\ H^\top R^{-1}H & I - \frac{h}{2}A^\top(\widehat{U}(jh)) \end{pmatrix} \begin{bmatrix} B(jh)V^{-1}(jh) \\ I \end{bmatrix}.\end{aligned} \tag{3.10}$$

In other words, the term $A(U)U$ of the continuous system is decoupled by setting $q(jh) = U(jh)$ in the discrete system (3.9): $A(q)U = A(U(jh))U(h(j+1))$. As $h \to 0$, $q(jh)$ gets closer to $U(j(h+1))$ and, in the limit, the solution of (3.9)-(3.10) should be converging to the solution of (3.7). In the following section this convergence is numerically assessed on two different examples.

4. Numerical experiments

We present two numerical examples illustrating the efficacy of the proposed data assimilation algorithm. The first example reconstructs the true solution, given the exact DG-SW model and incorrect initial conditions. Our second

example, reconstructs the true solution in the presence of state-dependent model error, i.e., an unknown Manning's coefficient. In what follows, we apply a second order DG method coupled with minimax filter as defined in (3.9). The gravitational constant g is fixed as $9.81 m/s^2$.

4.1. Uncertain initial condition

We first consider the benchmark 'ideal dam-break' problem [27] to verify the performance of DG method and the TVD property without data assimilation. For the ideal dam break problem, equations (2.1) are equipped with the following initial conditions:

$$u(x,0) = 0 \quad \text{and} \quad h(x,0) = \begin{cases} 1 & \text{if } 0 \le x \le 0.5 \\ 0.5 & \text{if } 0.5 < x \le 1, \end{cases} \tag{4.1}$$

and the reflective boundary conditions are imposed:

$$h(0,t) = h(0^+,t); \quad h(1,t) = h(1^-,t); \qquad u(0,t) = -u(0^+,t); \quad u(1,t) = -u(1^-,t)\,. \tag{4.2}$$

In this case, the term $ghBS_f$ is set to 0 so there is no model error. The width of the domain B is set to 1. We compute the solution until $t = .12$ using 40 uniform cells. The computed solution and the exact solution for h and hu are plotted in Fig. 4.1 and the plot shows that the method works as expected. We now consider the ideal dam break problem with the incorrect initial conditions for both h and hu: specifically, we consider random initial conditions generated by a smooth Perlin function. The observations are obtained from the exact solution of the ideal dam break problem at 5 uniformly distributed locations for both h and hu without adding any noise. The data assimilation algorithm is implemented according to the scheme (3.9)-(3.10).

Fig. 4.2 shows the comparison of the data assimilation algorithm versus the exact solution and the observations at times $t = 0, 0.02, 0.04, 0.08$. We observe that the minimax estimate converges to the true solution over time, and by $t = 0.12$ (1200 time steps) the estimate appears to have converged to the true solution and the shock and rarefaction locations are reconstructed accurately.

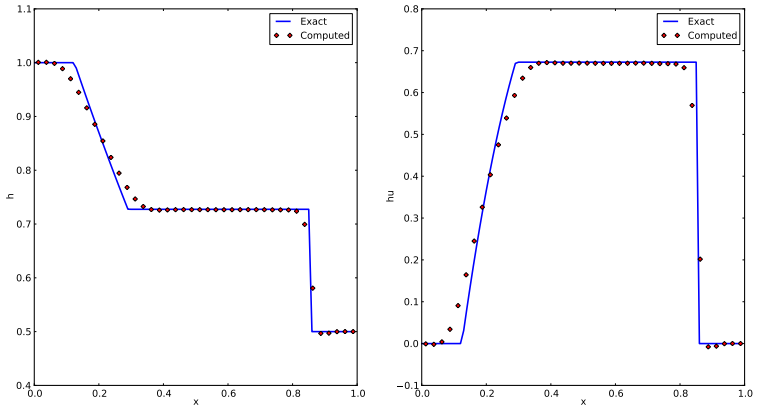

Fig. 4.1: Computed and exact solutions of h (left) and hu (right) at time $t = .12$ for the ideal dam break problem using 2^{nd} order DG elements and TVD limiters with 40 uniform cells.

We stress that the estimate uses just 5 sensors and the data provided by these sensors is not enough to track the shocks accurately by using a solely data driven approach as the model plays a crucial role here. In other words, the presence of the physical model DG-SW allows us to optimally interpolate the parts of the true solution which are not seen through the sensors. In addition, we note that the boundary conditions used by the minimax estimate are incorrect, that is the filter starts off from the wrong initial condition and so the corresponding solution is far from the true solution. As a result, the imposed reflective boundary conditions result in an incorrect source term in the DG discretization until the estimate gets close enough to the true solution at the boundaries.

We compare the performance of the minimax filter to Ensemble Kalman filter which is commonly used for state estimation and filtering in physical modeling [28]. There are various forms of EnKF used in practice and we follow the algorithm defined in [29, 28] for this comparison. In order to ensure a fair comparison, we run the EnKF filter using the same initial and boundary conditions and the same observations as for the minimax filter which is shown in Fig. 4.2. The EnKF results for 5 observations and 20 observations respectively using

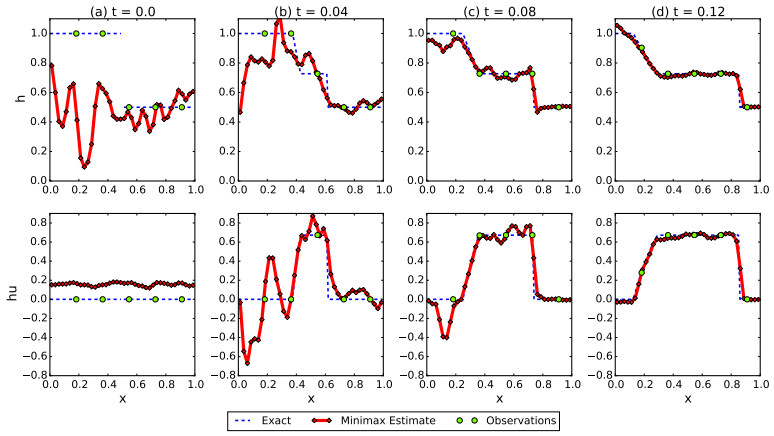

Fig. 4.2: Minimax estimate of h (top) and hu (bottom) using $Q = \mathbf{I}$, $S = 0.1\mathbf{I}$ and $R = 0.001\mathbf{I}$ with initial random noise generated through a Perlin function using 5 uniformly distributed observations.

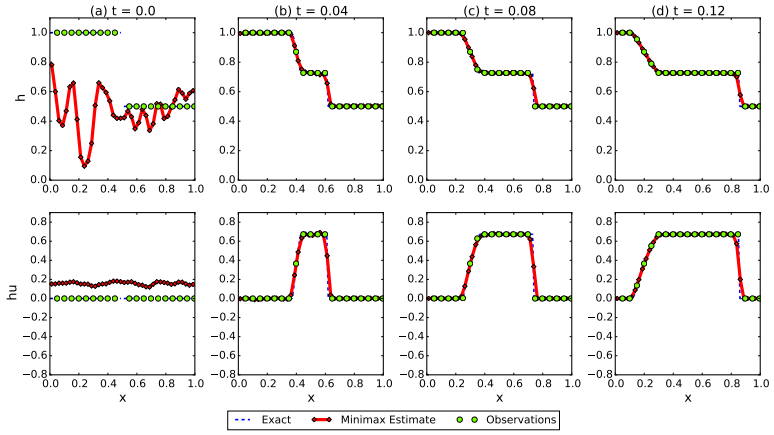

Fig. 4.3: Minimax estimate of h (top) and hu (bottom) using $Q = \mathbf{I}$, $S = 0.1\mathbf{I}$ and $R = 0.001\mathbf{I}$ with initial conditions same as Fig. 4.2 using 20 uniformly distributed observations.

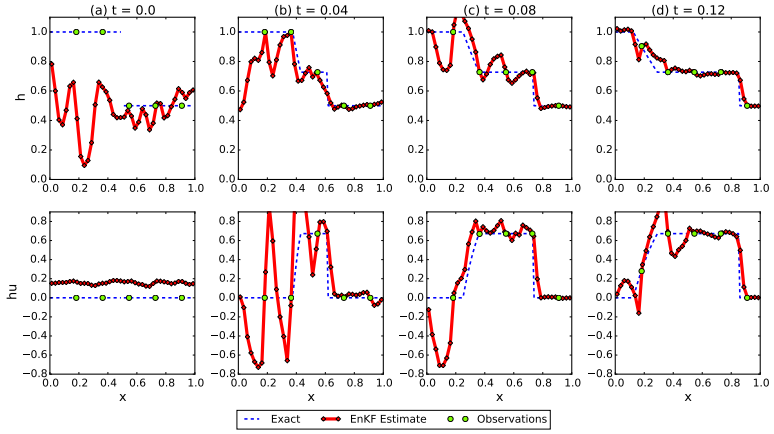

Fig. 4.4: EnKF estimate of h (top) and hu (bottom) using 160 ensemble members for the same initial conditions same as Fig. 4.2 using 5 uniformly distributed observations.

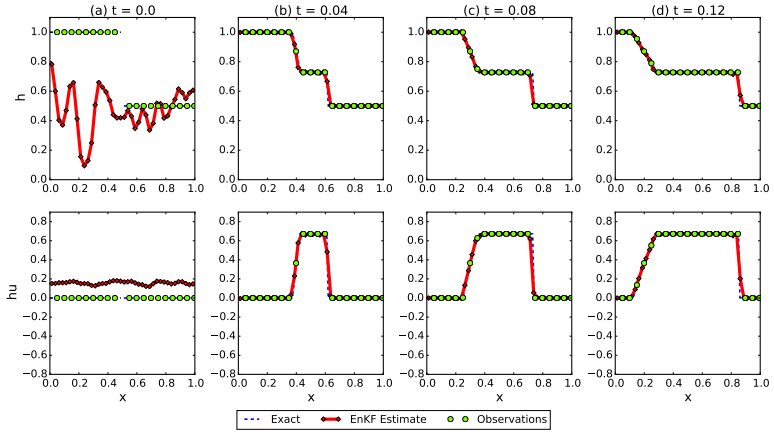

Fig. 4.5: EnKF estimate of h (top) and hu (bottom) using 160 ensemble members for the same initial conditions same as Fig. 4.2 using 20 uniformly distributed observations.

the same parameters (observation error covariance matrix: $\mathbf{W} = 0.001\mathbf{I} = R$ and initial model state covariance matrix: $\mathbf{P} = 0.1\mathbf{I} = S$, and model error: $\mathbf{Q_e} = \mathbf{I} = Q$) are shown in Fig. 4.4 and Fig. 4.5. It is important to note that the computational cost required to solve the system with minimax filter is approximately equal to that of solving the system with an EnKF filter consisting of 20 ensemble members in this case (Fig. 4.6). We however consider 160 ensemble members in this example to show the very slow convergence of EnKF filter to the ground truth with 5 observations (compared to the minimax filter) and the inability of the model to capture the rarefaction waves. On the other hand, the minimax filter performs well for 5 observations and improves the convergence with 20 observations (Fig. 4.3).

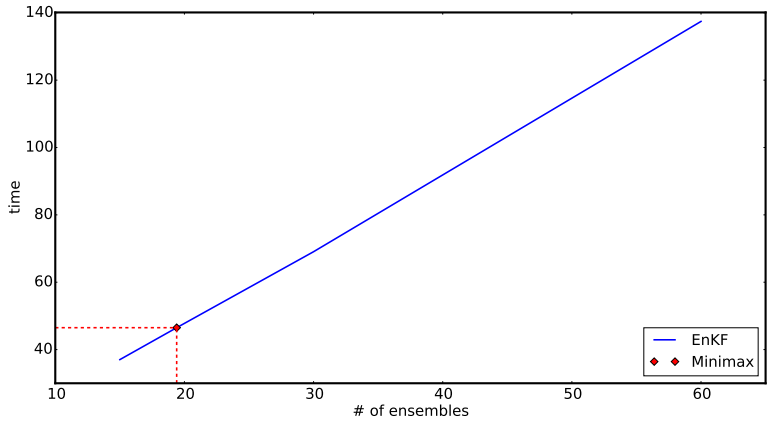

Fig. 4.6: Computational time for the EnKF filter with various number of ensemble members using 5 uniformly distributed observations (Intel(R) Core(TM) i7 − 3740QM CPU, 2.70GHz processor).

In what follows we discuss the performance of the filter, show dynamics of the estimation error (both in time and space) and study sensitivity of the filter to the choice of designer parameters S, Q, R with 10 observations and time-step of 0.001. As stated in section 3, the tunable parameters in the filtering model are R, S and Q matrices. Fig. 4.7 shows that the choice of the parameters strongly affect the accuracy of the solution. In this case, since there is a large

error in the initial conditions, a lower value of S is preferable to reflect the (lack of) trust in the initial conditions. R is set to I to allow the estimate to deviate from the observed data. Q is taken as an identity matrix since there is only numerical model error (projection error of DG method) and no physical model error.

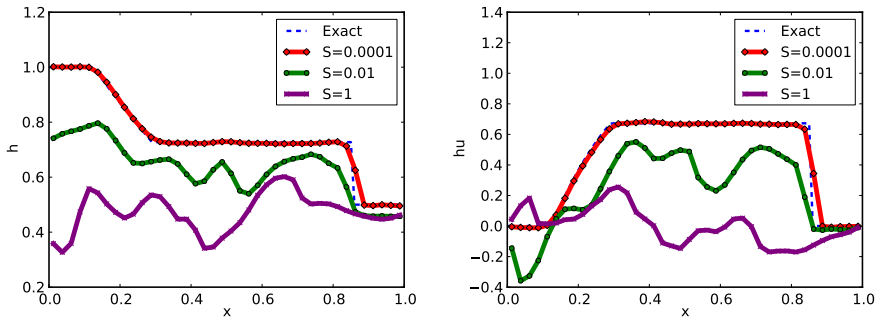

(a) h (b) hu

Fig. 4.7: Minimax estimate of h (left) and hu (right) with $Q = \mathbf{I}$, $R = \mathbf{I}$ where $\mathbf{I}$ is an identity matrix for various values of S at $t = 0.12$.

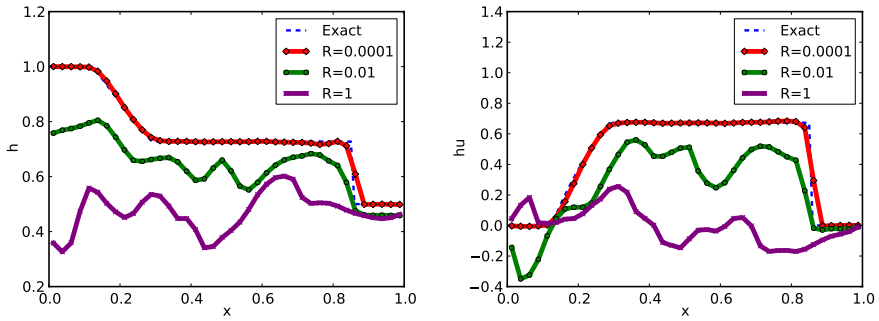

(a) h (b) hu

Fig. 4.8: Minimax estimate of h (left) and hu (right) with $Q = \mathbf{I}$, $S = \mathbf{I}$ where $\mathbf{I}$ is an identity matrix for various values of R at time $t = 0.12$.

The dependence of the minimax estimate on R is also tested based on the

exact observations taken at every time-step (see Fig. 4.8). In this case, S is taken as an identity matrix and the non-zero diagonal entries of the diagonal matrix R are reduced to reflect the increasing trust in the observations (namely, "small" R means that $\sum_i E\eta_i^2$ is "small" and so the realisations of the observation noise η are very likely to be close to $E\eta = 0$). As expected, the filter tracks the observed signal almost exactly for low R and it deviates from observations significantly as R increases (see Fig. 4.8). We next consider the case where

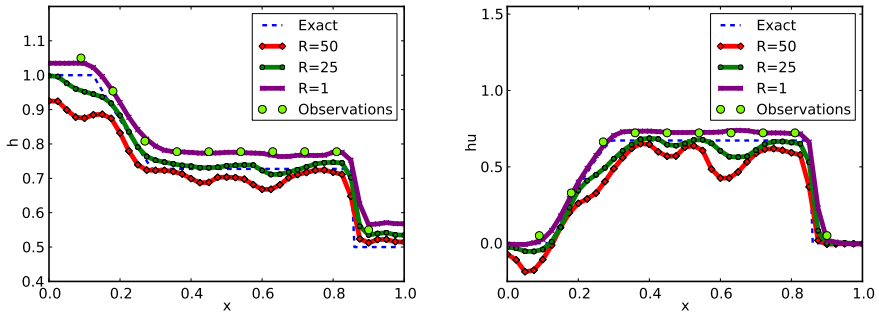

(a) h (b) hu

Fig. 4.9: Minimax estimate of h and hu with $Q = \mathbf{I}$, $S = 0.0001\mathbf{I}$ where $\mathbf{I}$ is an identity matrix for various values of R with errors in the observations at $t = 0.12$.

the observations are shifted from the true solution and again generate different estimates corresponding to the various values of R. Unlike the previous case, where the observations are the exact solutions and hence a small value of R is preferable, we need to increase the value of R to track the true solution. Fig. 4.9 shows that filter tracks the observed signal almost exactly and ignores the noise for low $R = 1$. In contrast, noise is better filtered out in the cases of $R = 25$.

Fig. 4.10 shows the error estimate of the minimax filter in space for two distinct time instants: $t = 0.02$ and $t = 0.08$. The error in space is computed as follows: $\ell^\top \widehat{U}(jh) \pm \ell^\top B(jh)V^{-1}(jh)\ell^{\frac{1}{2}}$ and ℓ runs through the canonical basis vectors $e_i = (0 \dots 1 \dots 0)^\top$. It is observed that the error bounds shrink over

time which is an indicator that the minimax solution is converging to the true solution. It can also be observed in Fig. 4.10 that at early times, the worst case error is lower near the observations which shows that faster convergence can be expected if the number of observations increases. Fig. 4.11 displays the

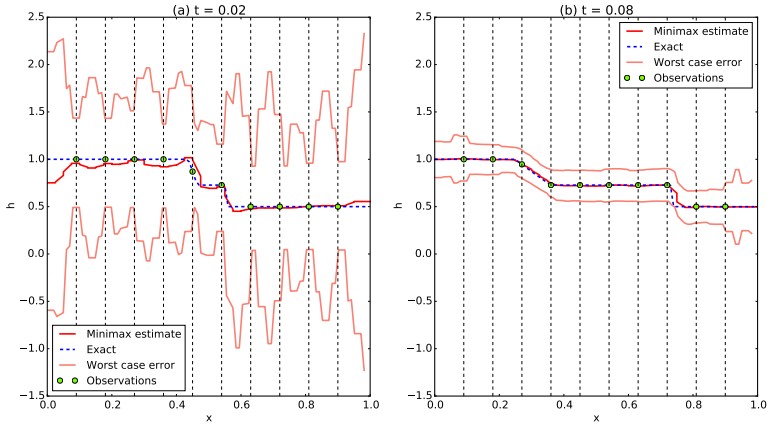

Fig. 4.10: Minimax estimate of h with error estimate at the observation points using $Q = \mathbf{I}$, $S = 0.1\mathbf{I}_N$ and $R = 0.001\mathbf{I}_M$ where $\mathbf{I}_{N(M)}$ is an identity matrix of size $N(M)$.

dynamics of the minimax estimate and minimax error for a fixed location in space where worst-case error stabilizes after the transition phase and does not decay further. In contrast, the estimate tracks the truth almost exactly through out the time period. As noted in section 3, the maximum eigenvalue of $A(U(t))$ in these examples is -3.24×10^{-9} that makes $P(A(U(jh)))$ well defined (see section 3.1).

4.2. Physical model error

In the next example, we consider the case of a hydraulic jump where super-critical flow changes to subcritical flow [30]. The governing equations in [30] are the modified shallow-water equations given by the one-dimensional Boussinesq

equations as:

$$\begin{cases} \dfrac{\partial hB}{\partial t} + \dfrac{\partial}{\partial x}\left(huB\right) = 0, \\ \dfrac{\partial (huB)}{\partial t} + \dfrac{\partial}{\partial x}\left(hu^2 + \dfrac{1}{2}gh^2B - \dfrac{1}{3}h^3E\right) = -ghBS_f, \end{cases} \tag{4.3}$$

where $E = \frac{\partial^2 u}{\partial x \partial t} + u\frac{\partial^2 u}{\partial x^2} - (\frac{\partial u}{\partial x})^2$.

Various numerical methods, including DG methods, have been developed to model hydraulic jumps by considering the complete equations or the simplified shallow water equations [30, 31, 32, 33, 34, 35]. It is well documented in these papers that the location of the shock is strongly dependent on the Manning's coefficient n (in the notation of section 2) and the numerical simulations use a trial and error approach by matching the computed water surface profile with the measured water level to determine the Manning's coefficient. In this example, we try to track the shock location in the presence of the physical model error which is caused by ignoring Boussinesq terms ($\frac{1}{3}h^3E$) and also by an unknown Manning's coefficient n. (Note: The governing equations (4.3) reduce to SWE provided the Boussinesq terms are ignored.). In this case, the data assimilation algorithm is implemented according to the scheme (3.9)-(3.10) and matrix Q starts to play an important role for the estimation quality. To accommodate state dependent model error we split $e(U)$ as follows: $e(U) = e(U, \bar{n}) + e(U, t)$ where $e(U, \bar{n})$ corresponds to an averaged value of the Manning's coefficient $n = \bar{n} = 0.0095$ and $e(U, t)$ is considered to be a fluctuation which is bounded and belongs to the ellipsoid (3.2) defined by S and Q. Numerical experiments show that our algorithm is robust, i.e. state estimation quality does not drop even in the presence of the state dependent model error $e(U, t)$.

We consider two test cases from [30] with upstream Froude numbers 2.3 and 7.0 and downstream Froude numbers given by .54 and .28 respectively. Manning's coefficient varies from $0.008s/m^{1/3}$ to $0.011s/m^{1/3}$ for the range of Froude numbers considered in these two test cases [30]. We consider the average value of $n = 0.0095s/m^{1/3}$ for both tests. Observation data is generated by solving the DG-SW model forward in time with the correct value of the

Manning's coefficient determined by trial and error as was done previously [32, 33]. The observation data for h and hu is generated at 10 locations for every time step until steady state is reached. The computational domain is given by $[0, 14] \times [0, 0.46]$ ($B = 0.46$). For the first case, the upstream velocity is $1.826m/s$, the upstream depth is $.064m$ and the downstream depth is $.168m$. For the second case, the upstream velocity is $3.831m$, the upstream depth $.031m$ and the downstream depth $.265m$. The prescribed boundary conditions are compatible with the supercritical flow at the upstream and subcritical flow at the downstream respectively [30]. The initial values for the water depth and velocity are considered to be the same as the upstream boundary conditions for both the test cases. 50 second order DG elements and a time step of .02 were used in this test. The matrices S, Q and R are taken as identity for this example.

The numerical solutions of water depth, momentum and the synthetic observations, at time $t = 40, 80, 120$ and 160 are shown in Fig. 4.12. The blue line indicates the solution without data assimilation and the red line with data assimilation for the same Manning's coefficient ($n = 0.0095$). Since the Manning's coefficient is larger than the actual value ($n \approx 0.008$ in this case), the jump travels from the downstream end to the upstream end and stabilizes closer to the upstream end as compared to the experimentally observed jump location. From these figures, we observe that the data assimilation method developed in this paper is able to absorb the wrong value of the Manning's coefficient and still propagate the location of the shock accurately (visually). The error brought by ignoring the Boussinesq terms is small relative to the other spatial derivative terms in the vicinity of the hydraulic jump ([30]) and consequently these terms result in a minor change in the location compared to the friction force.

Next, we compare the minimax estimate against real data (experimental observations) which is available only at one instant of time ($t = 160$) [30]. Fig. 4.13 shows the water surface profiles for the two test cases and the corresponding experimentally observed values. The blue lines (solid and dashed) are the numerical results with $n = 0.0095$ and various Froude numbers without data

assimilation., and the red lines represent the minimax estimates with the same n and Froude numbers. Again, we observe that the data assimilation algorithm solutions match the locations of the hydraulic jumps without special tuning of the value of Manning's coefficient and ignoring the Boussinesq terms for the both test cases. In this example the maximum eigenvalue of $A(U(t))$ is -1.24×10^{-9}.

Finally, the sensitivity of the shock location to the model error parameter Q is shown in Fig. 4.14. It can be seen that the choice of Q impacts the location of the hydraulic jump (R and S are taken as identity matrices for different values of Q).

5. Conclusions

In this paper, we developed a numerical model based on Discontinuous Galerkin (DG) method with data assimilation performed through minimax filters to solve the one-dimensional shallow water equations. A global stiffness matrix is assembled from the weak form of the discretized governing equations and this representation is used for data assimilation. The minimax estimate is post-processed with a TVD limiter to control spurious oscillations. The numerical scheme and the assimilation framework are evaluated by testing the model with incorrect initial conditions for an ideal dam break problem and studying the properties of hydraulic jump with simplified governing equations and using an approximate value for the Manning's coefficient. These test cases show that the data assimilation model with DG methods for shallow water equation is capable of modeling flows with unknown initial conditions and parameter values even with sparse observations. In addition, we observed that the minimax filter converges faster to the true solution as compared to EnKF for sparse observations. DG methods with data assimilation can further be potentially applied to solve shallow water equations for natural rivers. Data assimilation can prove to be very effective to minimize the errors resulting in the model because of the inaccuracies in profiling the cross-sectional area and the bottom topography. These applications and 2D extension of this method are part of the ongoing

work.

Acknowledgments

The authors would like to thank the reviewers for their valuable feedback.

References

[1] S. Néelz, G. Pender, et al., Benchmarking of 2D hydraulic modelling packages, Bristol: Environment Agency, 2010.

[2] C.-W. Shu, Essentially non-oscillatory and weighted essentially non-oscillatory schemes for hyperbolic conservation laws, Springer, 1998.

[3] G. Kesserwani, Y. Wang, Discontinuous Galerkin flood model formulation: Luxury or necessity?, Water Resources Research 50 (8) (2014) 6522–6541.

[4] X. Lai, J. Monnier, Assimilation of spatially distributed water levels into a shallow-water flood model. Part I: Mathematical method and test case, Journal of Hydrology 377 (1) (2009) 1–11.

[5] R. Hostache, X. Lai, J. Monnier, C. Puech, Assimilation of spatially distributed water levels into a shallow-water flood model. Part II: Use of a remote sensing image of mosel river, Journal of Hydrology 390 (3) (2010) 257–268.

[6] L. Giustarini, P. Matgen, R. Hostache, M. Montanari, D. Plaza, V. Pauwels, G. De Lannoy, R. D. Keyser, L. Pfister, L. Hoffmann, et al., Assimilating SAR-derived water level data into a hydraulic model: a case study, Hydrology and Earth System Sciences 15 (7) (2011) 2349–2365.

[7] O. P. Tossavainen, J. Percelay, A. Tinka, Q. Wu, A. M. Bayen, Ensemble Kalman filter based state estimation in 2d shallow water equations using Lagrangian sensing and state augmentation, in: Decision and Control, 2008. CDC 2008. 47th IEEE Conference on, IEEE, 2008, pp. 1783–1790.

[8] I. S. Strub, J. Percelay, O.-P. Tossavainen, A. M. Bayen, Comparison of two data assimilation algorithms for shallow water flows., NHM 4 (2) (2009) 409–430.

[9] C. Aricò, C. Nasello, T. Tucciarelli, Using unsteady-state water level data to estimate channel roughness and discharge hydrograph, Advances in Water Resources 32 (8) (2009) 1223–1240.

[10] C. Aricò, M. Sinagra, L. Begnudelli, T. Tucciarelli, Mast-2d diffusive model for flood prediction on domains with triangular delaunay unstructured meshes, Advances in Water Resources 34 (11) (2011) 1427–1449.

[11] Y. Xing, X. Zhang, C.-W. Shu, Positivity-preserving high order well-balanced discontinuous Galerkin methods for the shallow water equations, Advances in Water Resources 33 (12) (2010) 1476–1493.

[12] I. Gihman, A. Skorokhod, Introduction to the theory of random processes, Dover Books on Mathematics, Dover, 1997.

[13] J. Frank, S. Zhuk, Symplectic Möbius integrators for LQ optimal control problems, in: Proc. IEEE Conference on Decision and Control, 2014.

[14] S. Noelle, Y. Xing, C.-W. Shu, High-order well-balanced schemes, Numerical Methods for Balance Laws. Quaderni di Matematica 24 (2010) 1–66.

[15] Y. Xing, C.-W. Shu, A new approach of high order well-balanced finite volume weno schemes and discontinuous galerkin methods for a class of hyperbolic systems with source terms, Comput. Phys 1 (1) (2006) 100–134.

[16] D. I. Ketcheson, C. B. Macdonald, S. Gottlieb, Optimal implicit strong stability preserving Runge-Kutta methods, Applied Numerical Mathematics 59 (2) (2009) 373–392.

[17] S. Zhuk, J. Frank, I. Herlin, R. Shorten, Data assimilation for linear parabolic equations: minimax projection method, SIAM J. Sci. Comp.To appear.

[18] S. Zhuk, Estimation of the states of a dynamical system described by linear equations with unknown parameters, Ukrainian Math. J. 61 (2) (2009) 214–235.

[19] R. Iman, J. Helton, An investigation of uncertainty and sensitivity analysis techniques for computer models, Risk Analysis 8 (1) (1988) 71–90.

[20] F. L. Chernousko, State Estimation for Dynamic Systems, Boca Raton, FL: CRC, 1994.

[21] A. Kurzhanski, I. Vályi, Ellipsoidal calculus for estimation and control, Systems & Control: Foundations & Applications, Birkhäuser Boston Inc., Boston, MA, 1997.

[22] A. Nakonechny, A minimax estimate for functionals of the solutions of operator equations, Arch. Math. (Brno) 14 (1) (1978) 55–59.

[23] S. Zhuk, Minimax state estimation for linear discrete-time differential-algebraic equations, Automatica J. IFAC 46 (11) (2010) 1785–1789.

[24] S. Zhuk, Kalman duality principle for a class of ill-posed minimax control problems with linear differential-algebraic constraints, Applied Mathematics and Optimisation 68 (2) (2013) 289–309.

[25] S. Zhuk, T. Tchrakian, Parameter estimation for Euler equations with uncertain inputs, in: Proc. IEEE Conference on Decision and Control, 2015, `http://researcher.watson.ibm.com/researcher/files/ie-sergiy.zhuk/paper_SZ_TT_cdc15.pdf`.

[26] T. Tchrakian, S. Zhuk, A macroscopic traffic data assimilation framework based on Fourier-Galerkin method and minimax estimation, IEEE Transactions on Intelligent Transportation Systems (99) (2014) 1–13, special issue.

[27] J. J. Stoker, Water waves: The mathematical theory with applications, Vol. 36, John Wiley & Sons, 2011.

[28] G. Evensen, The ensemble Kalman filter: Theoretical formulation and practical implementation, Ocean dynamics 53 (4) (2003) 343–367.

[29] G. Burgers, P. Jan van Leeuwen, G. Evensen, Analysis scheme in the ensemble Kalman filter, Monthly Weather Review 126 (6) (1998) 1719–1724.

[30] A. M. Gharangik, M. H. Chaudhry, Numerical simulation of hydraulic jump, Journal of Hydraulic Engineering 117 (9) (1991) 1195–1211.

[31] A. Baghlani, N. Talebbeydokhti, M. J. Abedini, A shock-capturing model based on flux-vector splitting method in boundary-fitted curvilinear coordinates, Applied Mathematical Modelling 32 (3) (2008) 249–266.

[32] X. Ying, S. S. Wang, A new approach for implementing the HLL approximate riemann solver for one-dimensional dam-break flows, Proceedings of the Seventh International Conference on Hydroscience and Engineering (2006).

[33] D. Liang, R. A. Falconer, B. Lin, Comparison between TVD-MacCormack and adi-type solvers of the shallow water equations, Advances in Water Resources 29 (12) (2006) 1833–1845.

[34] M. Venutelli, A third-order explicit central scheme for open channel flow simulations, Journal of Hydraulic Research 44 (3) (2006) 402–411.

[35] W. Lai, A. A. Khan, Discontinuous Galerkin method for 1d shallow water flows in natural rivers, Engineering Applications of Computational Fluid Mechanics 6 (1) (2012) 74–86.

Appendix

To represent the weak form in matrix notation, we denote the integrals in 2.8 as,

$$M_{ik}^{j} = \int_{D^j} v_i(x) v_k(x) dx, \quad S_{ik}^{j} = \int_{D^j} v_i(x) \frac{dv_k(x)}{dx} dx\,, \tag{5.1}$$

and hence 2.8 can be rewritten as:

$$M^j \frac{dU}{dt} - (S^j)f = -\hat{f}(x_{j+\frac{1}{2}})v(x^-_{j+\frac{1}{2}}) + \hat{f}(x_{j-\frac{1}{2}})v(x^-_{j-\frac{1}{2}})\,. \tag{5.2}$$

Eq. 5.2, is assembled into a global matrix formulation for data assimilation. For this, Eq. 5.2, can be written in matrix form as:

$$\begin{pmatrix} M & 0 \\ 0 & M \end{pmatrix} \frac{d}{dt} \begin{pmatrix} \hat{h} \\ \hat{hu} \end{pmatrix} = \begin{pmatrix} A_{11} & A_{12} \\ A_{21} & A_{22} \end{pmatrix} \begin{pmatrix} \hat{h} \\ \hat{hu} \end{pmatrix} + \begin{pmatrix} b_h \\ b_{hu} \end{pmatrix} \tag{5.3}$$

where,

$$A_{11} = F^{h,h},\;\; A_{12} = F^{h,hu} + S^{h,hu},\;\; A_{21} = S^{hu,h} + F^{hu,h},\;\; A_{22} = S^{hu,hu} + F^{hu,hu}. \tag{5.4}$$

and $\hat{h}$ and $\hat{hu}$ are the modal coefficients in the approximate solutions.

$$\begin{aligned}
S^{h,hu}_{ik} &= (\partial_x v_i, v_k)_{\Omega_h}\,, \\
S^{hu,hu}_{ik} &= (\partial_x v_i, u_k)_{\Omega_h}\,, \\
S^{hu,h}_{ik} &= (\partial_x v_i, 0.5gh)_{\Omega_h}\,, \\
F^{h,h}_{ik} &= -.5\alpha \sum_j \{v_i|_{\partial D^j -}(v_k\chi)|_{\partial D^j -} + \{v_i|_{\partial D^j +}(v_k\chi)|_{\partial D^j +}\}\}\,, \\
F^{h,hu}_{ik} &= .5 \sum_j \{-v_i|_{\partial D^j -}(v_k)|_{\partial D^j -} + \{v_i|_{\partial D^j +}(v_k\chi)|_{\partial D^j +}\}\}\,, \\
F^{hu,h}_{ik} &= .5g \sum_j \{-v_i|_{\partial D^j -}(hv_k)|_{\partial D^j -} + \{v_i|_{\partial D^j -}(hv_k)|_{\partial D^j -}\}\}\,, \\
F^{hu,hu}_{ik} &= .5 \sum_j \{-v_i|_{\partial D^j -}(uv_k)|_{\partial D^j -} + \{v_i|_{\partial D^j +}(uv_k)|_{\partial D^j +}\}\} \\
&\quad -.5\alpha \sum_j \{v_i|_{\partial D^j -}(v_k\chi)|_{\partial D^j -} + \{v_i|_{\partial D^j +}(v_k\chi)|_{\partial D^j +}\}\}\,, \\
M_{ik} &= (v_i, v_k)_{\Omega_h}, \\
(e(U))_i &= (v_i, ST^n)_{\Omega_h}\,,
\end{aligned}$$

where, ST^n is defined by (2.5) and χ is given by:

$$\chi = \begin{cases} -1, & \text{if basis function is in the same cell as test function} \\ 1, & \text{otherwise} \end{cases}$$

$A = \begin{pmatrix} M & 0 \\ 0 & M \end{pmatrix}^{-1} \begin{pmatrix} A_{11} & A_{12} \\ A_{21} & A_{22} \end{pmatrix}$. This gives us the required form for data assimilation, given as:

$$\frac{dU}{dt} = A(U)U + e(U) + b(t). \tag{5.5}$$

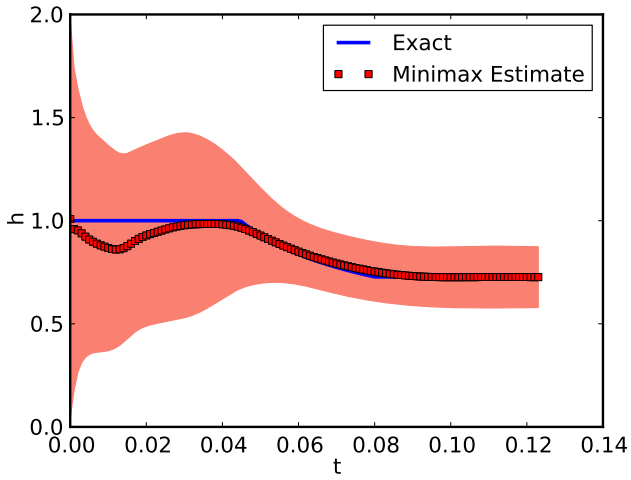

Fig. 4.11: Minimax estimate of h at the observation point $x = .364$ over time using $Q = \mathbf{I}$, $S = 0.1\mathbf{I}_N$ and $R = 0.001\mathbf{I}_M$ where $\mathbf{I}_{N(M)}$ is an identity matrix of size $N(M)$. The filled region is the worst-case error.

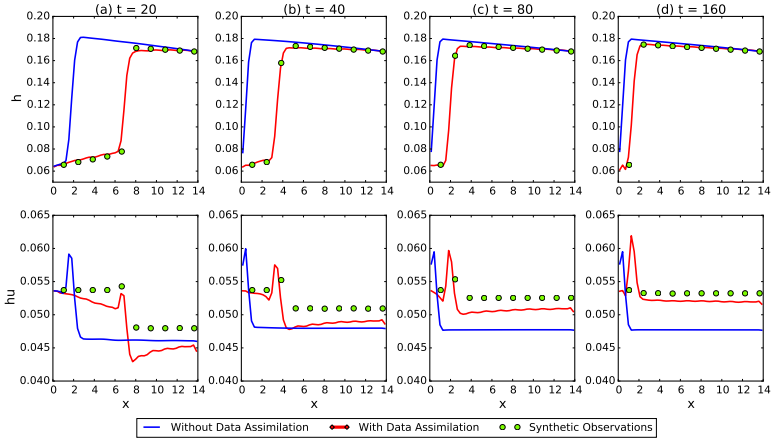

Fig. 4.12: Time evolution of the minimax estimate of h (top) and hu (bottom). From left to right, $t = \{40, 80, 120, 160\}$.

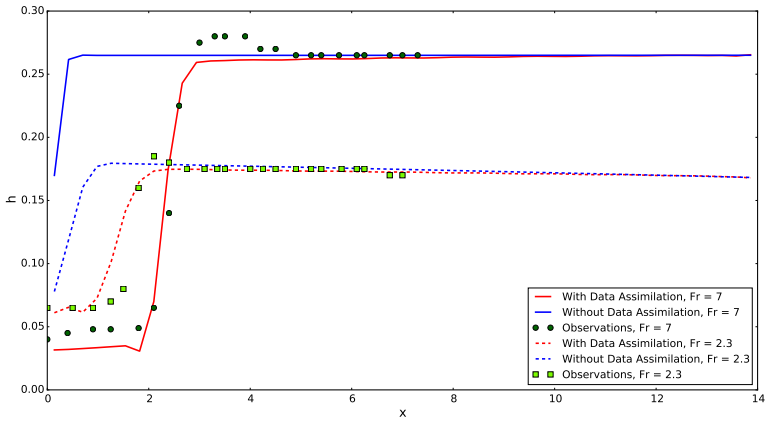

Fig. 4.13: Minimax computed water surface profiles with the experimentally observed data for the two test cases with $Fr = 7$ (solid lines) and $Fr = 2.3$ (dashed lines) respectively [30].

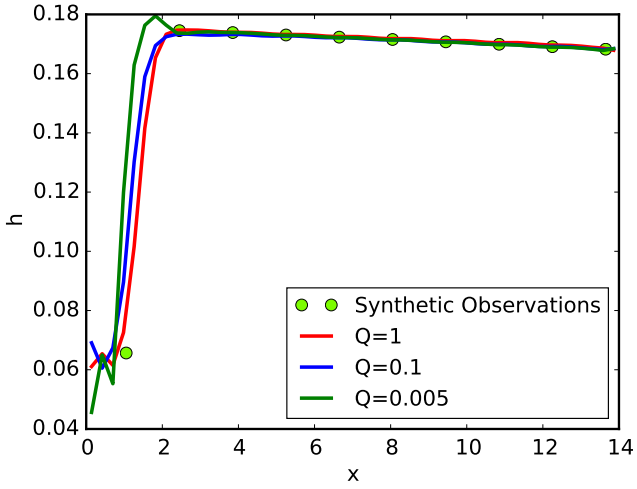

Fig. 4.14: Dependence of the minimax estimate of h on Q. $S = \mathbf{I}$ and $R = \mathbf{I}$ where $\mathbf{I}$ is an identity matrix.